Research Square

Preprints are preliminary reports that have not undergone peer review.
They should not be considered conclusive, used to inform clinical practice,
or referenced by the media as validated information.

Incremental Value of Pretreatment 18F-FAPI PET/CT and MRI for Predicting Early Treatment Response and Long-Term Prognosis in Nasopharyngeal Carcinoma Undergoing Chemoradiotherapy

Lingling Gao
Yongkang First People's Hospital of Wenzhou Medical University
Rui Yao
the First Affiliated Hospital of Wenzhou Medical University
Xiaolong Zheng
Yongkang First People's Hospital of Wenzhou Medical University
Yujia Zhang
the First Affiliated Hospital of Wenzhou Medical University
Qingyou Ye
the First Affiliated Hospital of Wenzhou Medical University
Xinyan Zhang
the First Affiliated Hospital of Wenzhou Medical University
Ling Wang
the First Affiliated Hospital of Wenzhou Medical University
Kun Tang
kuntang007@163.com

the First Affiliated Hospital of Wenzhou Medical University https://orcid.org/0000-0003-0996-0481

Research Article

Keywords: nasopharyngeal carcinoma, 18F-labeled fibroblast activation protein inhibitor positron emission tomography/computed tomography (18F-FAPI PET/CT), magnetic resonance imaging (MRI), treatment response assessment, prognosis

Posted Date: November 5th, 2026

DOI: https://doi.org/10.21203/rs.3.rs-11408620/v1

License: This work is licensed under a Creative Commons Attribution 4.0 International License.
Read Full License

Title Page

Incremental Value of Pretreatment ^{18}F-FAPI PET/CT and MRI for Predicting Early Treatment Response and Long-Term Prognosis in Nasopharyngeal Carcinoma Undergoing Chemoradiotherapy

Lingling Gao [a], Rui Yao [b], Xiaolong Zheng [a], Yujia Zhang [b], Qingyou Ye [c], Xinyan Zhang [c], Ling Wang [b,d], Kun Tang [b,e,f]

[a] Department of Radiology, Yongkang First People's Hospital of Wenzhou Medical University, Jinhua, 321300, Zhejiang, China.

[b] Department of Nuclear Medicine, the First Affiliated Hospital of Wenzhou Medical University, Wenzhou, 325015, Zhejiang, China.

[c] Department of Radiology, the First Affiliated Hospital of Wenzhou Medical University, Wenzhou, 325015, Zhejiang, China.

[d] Key Laboratory of Clinical Laboratory Diagnosis and Translational Research of Zhejiang Province, The First Affiliated Hospital of Wenzhou Medical University, Wenzhou, 325015, Zhejiang, China.

[e] Key Laboratory of Intelligent Treatment and Life Support for Critical Diseases of Zhejiang Province, Wenzhou, 325015, Zhejiang, China.

[f] Key Laboratory of Novel Nuclide Technologies on Precision Diagnosis and Treatment & Clinical Transformation of Wenzhou City, Wenzhou, 325015, Zhejiang, China.

Corresponding author:

Kun Tang, MD, PhD.

Department of Nuclear Medicine, The First Affiliated Hospital of Wenzhou Medical University, Nanbaixiang Street, Ouhai District, Wenzhou 325015, China; Key Laboratory of Intelligent Treatment and Life Support for Critical Diseases of Zhejiang Province, Wenzhou, China; Key Laboratory of Novel Nuclide Technologies on Precision Diagnosis and Treatment & Clinical Transformation of Wenzhou City, Wenzhou, China.

Email: kuntang007@163.com.

Telephone: +86 13777785264

Incremental Value of Pretreatment ^{18}F-FAPI PET/CT and MRI for Predicting Early Treatment Response and Long-Term Prognosis in Nasopharyngeal Carcinoma Undergoing Chemoradiotherapy

Abstract

Objectives: Effective noninvasive tools for predicting treatment response and prognosis in nasopharyngeal carcinoma (NPC) remain lacking. This study aimed to investigate the predictive value of integrating pretreatment ^{18}F-fibroblast activation protein inhibitor positron emission tomography/computed tomography (^{18}F-FAPI PET/CT) and magnetic resonance imaging (MRI) for short-term complete response (CR) and progression-free survival (PFS) in patients with NPC undergoing chemoradiotherapy.

Materials and Methods: This retrospective study analyzed pretreatment ^{18}F-FAPI PET/CT and contrast-enhanced MRI (CE-MRI) parameters in 46 patients with NPC who underwent chemoradiotherapy. Logistic regression identified predictors of CR and developed predictive models, which were evaluated using receiver operating characteristic (ROC) curves, DeLong test, bootstrap internal validation, and decision curve analysis (DCA). Cox regression identified independent predictors of PFS, while Kaplan–Meier analysis and log-rank test evaluated survival outcomes.

Results: Nineteen patients (41.3%) achieved CR, whereas 27 (58.7%) did not. Total lesion fibroblast activation protein expression (TLF), signal intensity ratio (SIR), and radiologic extranodal extension (rENE) independently predicted CR. A multimodal model incorporating these variables achieved an area under the curve (AUC) of 0.88,

outperforming PET/CT-only (AUC = 0.76) and MRI-only (AUC = 0.79) models numerically. A maximum standardized uptake value of the primary lesion (SUVmax-T) ≥ 17.0 and the presence of rENE independently predicted shorter PFS. The Sankey diagram illustrated that high-risk parameter combinations were associated with non-CR and shorter PFS, while short-term CR was strongly concordant with longer PFS.

Conclusion: Pretreatment ^{18}F-FAPI PET/CT and MRI provide complementary information that may improve short-term response assessment and prognostic stratification in NPC.

Key words: nasopharyngeal carcinoma; ^{18}F-labeled fibroblast activation protein inhibitor positron emission tomography/computed tomography (^{18}F-FAPI PET/CT); magnetic resonance imaging (MRI); treatment response assessment; prognosis

Introduction

Nasopharyngeal carcinoma (NPC) is a malignant tumor originating from the epithelial cells of the nasopharynx and exhibits a marked geographic distribution, with a high incidence in southern China and Southeast Asia [1]. Owing to the deep anatomical location of the nasopharynx and the subtlety of early symptoms, approximately 70% of patients have locally advanced disease at diagnosis [2], concurrent chemoradiotherapy is the primary treatment strategy for these patients [3]. However, treatment outcomes vary substantially among patients, and several clinical challenges remain. Effective noninvasive approaches for predicting treatment response before therapy are currently lacking. Consequently, high-risk patients—such as those with residual local disease after treatment or a predisposition to early distant metastasis—are difficult to identify at an early stage, potentially resulting in missed opportunities for intensified intervention. Although the TNM staging system and biomarkers such as EBV DNA load provide prognostic information, their ability to predict treatment response remains limited [4,5]. Therefore, there is an urgent clinical need for noninvasive imaging tools capable of enabling accurate risk stratification.

^{18}F-Fluorodeoxyglucose positron emission tomography/computed tomography (^{18}F-FDG PET/CT) is the most widely used molecular imaging technique in oncology. However, its application in NPC is limited by interference from inflammatory responses and physiological glucose uptake in the brain. ^{18}F-labeled fibroblast activation protein inhibitors (^{18}F-FAPI) are a class of rapidly emerging tracers targeting fibroblast

activation protein (FAP). FAP is highly expressed in cancer-associated fibroblasts (CAFs) across a variety of malignancies, including NPC [6,7]. Through the secretion of various cytokines, growth factors, and matrix-remodeling enzymes, CAFs are closely involved in tumor invasion, metastasis, and therapeutic resistance [8]. Compared with ^{18}F-FDG, ^{18}F-FAPI offers lower background uptake and higher image contrast, providing advantages in NPC detection, staging, and target-volume delineation [9,10]. Nevertheless, PET/CT remains limited in delineating precise anatomical boundaries and assessing the depth of tumor infiltration. Magnetic resonance imaging (MRI), with its excellent soft-tissue contrast and sensitivity to lesion enhancement characteristics, can effectively compensate for these limitations. The combination of both modalities enables simultaneous characterization of the tumor microenvironment, anatomical structure, and vascularity, thereby providing a more comprehensive basis for treatment-response assessment [11].

However, the value of combining pretreatment ^{18}F-FAPI PET/CT and MRI to simultaneously predict short-term treatment response and progression-free survival (PFS) in patients with NPC undergoing chemoradiotherapy remains underexplored. Therefore, this study aimed to identify noninvasive imaging markers derived from pretreatment multimodal imaging parameters for prognostic stratification and to support individualized treatment decision-making.

1. Materials and Methods

1.1 Study Population

We retrospectively enrolled 86 patients with NPC who underwent ^{18}F-FAPI PET/CT at a university-affiliated hospital between January 1, 2024, and January 31, 2026. The inclusion criteria were as follows: (1) primary NPC confirmed by biopsy pathology; (2) all patients underwent ^{18}F-FAPI PET/CT and MRI before treatment, with an interval of no more than 7 days between the two examinations; (3) all patients completed chemoradiotherapy after the imaging examinations. The exclusion criteria were as follows: (1) receipt of radiotherapy, chemotherapy, targeted therapy, immunotherapy, or other antitumor treatment before PET/CT or MRI; (2) the presence of other primary malignancies; (3) severe cardiac, hepatic, or renal dysfunction; (4) incomplete clinical or imaging data; and (5) poor-quality PET/CT or MRI images that were inadequate for quantitative measurement. Based on these inclusion and exclusion criteria, 46 patients were ultimately considered eligible for the study (Figure 1). This study was conducted in accordance with the Declaration of Helsinki, as revised in 2013, and was approved by the Institutional Review Board of the participating institution (approval details masked for blind review). Given the retrospective nature of the study, the requirement for informed consent was waived.

1.2 Methods

1.2.1 PET/CT and MRI Examinations

^{18}F-AlF-NOTA-FAPI-04 PET/CT Tracer

^{18}F-AIF-NOTA-FAPI-04 (hereafter referred to as ^{18}F-FAPI) was produced using an in-house MINItrace cyclotron (GE Healthcare, USA). The radiochemical purity was > 95%.

PET/CT Examination

^{18}F-FAPI was administered intravenously at a dose of 0.10–0.12 mCi/kg. Approximately 60 min after injection, whole-body PET/CT imaging was performed using a uMI Panorama 35S scanner (United Imaging Healthcare, Shanghai, China). The scanning range extended from the vertex of the skull to the middle-to-upper thighs. Low-dose CT was performed first using the following parameters: tube voltage, 120 kV; automatic modulation of the effective tube current; pitch, 0.9625; tube rotation time, 0.5 s; slice thickness, 4.0 mm; and slice gap, 2.0 mm. PET data were subsequently acquired in three-dimensional mode, with an acquisition time of 2 min per bed position. The PET acquisition and reconstruction parameters were as follows: three iterations, 10 subsets, a Gaussian full width at half maximum of 3.0 mm, a matrix size of 256 × 256, and a field of view of 600 mm. PET images were reconstructed after CT-based attenuation correction and iterative reconstruction using the ordered-subsets expectation maximization algorithm. All data were transferred to the UWS-MI workstation (version 5.2.1; United Imaging Healthcare, Shanghai, China) for processing. PET, CT, and fused PET/CT images were subsequently reconstructed.

MRI Examination

MRI examinations were performed using a 3.0T MRI scanner (Achieva; Philips, the Netherlands). Routine noncontrast MRI of the nasopharyngeal region was performed first, followed by contrast-enhanced imaging after intravenous administration of gadopentetate dimeglumine at a dose of 0.1 mmol/kg. The noncontrast MRI protocol included axial T1-weighted imaging (T1WI), axial T2-weighted imaging (T2WI), and sagittal T1WI sequences. The imaging parameters were as follows: T1WI, repetition time (TR) = 2,000 ms and echo time (TE) = 20 ms; T2WI, TR = 3,000 ms and TE = 80 ms. The slice thickness was 4 mm, the slice gap was 0.4 mm, the field of view (FOV) was 220 × 220 mm, and the matrix size was 276 × 205. Contrast-enhanced imaging included axial, coronal, and sagittal T1WI sequences, using the same imaging parameters as those used for the noncontrast examination.

1.2.2 Image Analysis

PET/CT and MRI images were independently reviewed by two experienced nuclear medicine physicians and two experienced radiologists, respectively. In cases of disagreement, a consensus was reached through discussion.

PET/CT image analysis was performed using the FusionViewer software on the MedEx workstation (Medex Technology, Beijing, China). Lesion regions of interest (ROIs) were automatically delineated using 40% of the maximum standardized uptake value (SUVmax) as the threshold and were subsequently corrected manually. The following metabolic parameters were obtained: the maximum standardized uptake value of the primary nasopharyngeal lesion (SUVmax-T), FAPI-avid tumor volume (FTV),

total lesion fibroblast activation protein expression (TLF), and the maximum standardized uptake value of metastatic lymph nodes (SUVmax-N).

MRI image analysis was performed using INFINITT PACS. The area showing the most pronounced enhancement within the solid component of the tumor was selected, while blood vessels and necrotic areas were avoided. ROIs were delineated on the noncontrast and contrast-enhanced T1WI and designated as SI_0 and SI_1, respectively. On the same slice of the contrast-enhanced images, the medial pterygoid muscle on the unaffected side was identified. An ROI was placed in the central portion of the muscle while avoiding peripheral fatty spaces and small blood vessels, and this measurement was designated as SI_2. The area of each ROI was approximately 10–15 mm^2. Measurements were obtained three times for both the lesion and the muscle, and the mean values were used for analysis. The following parameters were recorded: the maximum diameter of the primary nasopharyngeal lesion (Max D), relative signal enhancement rate (RE), signal intensity ratio (SIR), radiologic extranodal extension in metastatic lymph nodes (rENE), and the T and N stages.

RE and SIR were calculated using the following formulas [12,13]:

$$\mathrm{RE}(\%) = \frac{\mathrm{SI}_1 - \mathrm{SI}_0}{\mathrm{SI}_0} \times 100\%$$

$$\mathrm{SIR} = \frac{\mathrm{SI}_1}{\mathrm{SI}_2}$$

1.2.3 Treatment and Follow-up

All patients received induction chemotherapy before undergoing intensity-modulated radiotherapy (IMRT). The chemotherapy regimens consisted of liposomal paclitaxel or gemcitabine combined with cisplatin or carboplatin. Radiotherapy was initiated after 2–4 cycles of chemotherapy. The total prescribed radiation dose was 68–70 Gy, delivered in 30–33 fractions.

Short-term treatment response assessment: All patients underwent reassessment 3 months after completion of chemoradiotherapy according to the Response Evaluation Criteria in Solid Tumors, version 1.1 (RECIST 1.1) [14]. Patients were classified into a complete response (CR) group, defined as the disappearance of all target lesions, and a non-complete response (Non-CR) group, defined as the presence of any residual lesions, including the primary tumor or metastatic lymph nodes, or the appearance of new lesions. The Non-CR group included patients with partial response (PR), stable disease (SD), or progressive disease (PD).

Long-term treatment outcome assessment: The follow-up endpoint was PFS, defined as the time from the initiation of induction chemotherapy to disease progression or death from any cause. The date of the last follow-up was June 30, 2026. Patients who had not experienced a PFS event by the date of the last follow-up were censored at that time.

1.3 Statistical Analysis

The normality of continuous variables was assessed using the Shapiro–Wilk test. Normally distributed variables are presented as the mean ± standard deviation (SD), and

between-group differences were assessed using the independent-samples t test. Non-normally distributed variables are presented as the median and interquartile range (IQR), and between-group differences were assessed using the Mann–Whitney U test. Categorical variables are expressed as frequencies and percentages and were compared between groups using the chi-square test or Fisher's exact test, as appropriate.

Spearman correlation analysis was used to assess correlations between variables. When two or more variables showed a correlation coefficient of $r > 0.90$, the variables were carefully evaluated and only the most clinically relevant variable was retained. Variables with $P < 0.10$ in univariable logistic regression analysis were entered into multivariable logistic regression models constructed using backward stepwise selection. The predictive performance of each model was evaluated using receiver operating characteristic (ROC) curves. The areas under the ROC curves (AUCs) were compared pairwise using DeLong's test. Internal validation was performed using bootstrap resampling. Calibration curves were used to assess model calibration, and decision curve analysis (DCA) was performed to evaluate the clinical utility of each model.

Optimal cutoff values for the continuous variables were determined using ROC curves, and the corresponding AUCs were calculated. Variables with an AUC < 0.60 or those resulting in complete separation after categorization according to the optimal cutoff value were categorized using their median values instead. Univariable and multivariable Cox proportional hazards regression analyses were performed to identify independent risk factors for PFS. Survival curves were generated using the Kaplan–

Meier method, and differences in survival between groups were assessed using the log-rank test.

All analyses were performed using SPSS version 27.0.1 (IBM Corp., Armonk, NY, USA) and R version 4.3.3 (R Foundation for Statistical Computing, Vienna, Austria). Two-sided P values < 0.05 indicated statistically significant differences.

2 Results

2.1 Patient Characteristics and Follow-up Outcomes

The baseline characteristics of the 46 patients are summarized in *Table 1*. There were 28 male patients (60.9%) and 18 female patients (39.1%), with a median age of 55 years (IQR, 42–65 years). Histopathological examination confirmed nonkeratinizing squamous cell carcinoma in all patients.

At the 3-month post-treatment assessment, 19 patients achieved a CR, 25 achieved a PR and 2 had PD. The median follow-up duration was 16.6 months (IQR, 9.7–22.4 months). During follow-up, disease progression occurred in 7 patients (15.2%); 2 patients (4.3%) died and 5 patients (10.9%) developed metastases. The PFS rates for the entire cohort were 97.8% at 6 months, 85.2% at 12 months, and 82.1% at 18 months.

2.2 Short-term Treatment Response

2.2.1 Comparison Between the Two Groups

A total of 46 patients were included in this study, including 19 (41.30%) with CR and 27 (58.70%) with Non-CR. Significant between-group differences were observed in SUVmax-T, FTV, TLF, SUVmax-N, MRI N stage, and rENE (P < 0.05), whereas no

significant differences were observed in age, sex, TNM stage, MRI T stage, Max D, SIR, or RE ($P > 0.05$; *Table 1*).

Spearman correlation analysis demonstrated a strong correlation between FTV and TLF ($r = 0.915$, $P < 0.0001$). Because TLF incorporates both the volume of FAPI-avid lesions and the intensity of FAP-targeted tracer uptake, it provides a more comprehensive assessment of whole-body FAP-expressing tumor burden. Accordingly, FTV was excluded from the multivariable analysis, and only TLF was retained to minimize potential collinearity.

2.2.2 Model Development and Evaluation of Predictive Performance

Variables with $P < 0.1$ in the univariable analyses were entered into a multivariable logistic regression model. Backward stepwise regression was then performed to identify independent predictors. The results showed that TLF, SIR, and rENE were independent predictors of achieving CR in patients with NPC after treatment ($P < 0.05$; *Table 2*).

Based on these findings, PET/CT-based, MRI-based, and combined predictive models were developed to discriminate short-term treatment response in patients with NPC. The combined model yielded an AUC of 0.88 (95% confidence interval [CI], 0.77–0.98), an accuracy of 0.83 (95% CI, 0.69–0.92), a sensitivity of 0.84 (95% CI, 0.68–1.00), and a specificity of 0.81 (95% CI, 0.67–0.96). DeLong's test showed that although the AUC of the combined model was numerically higher than those of the PET/CT-based model (AUC = 0.76) and the MRI-based model (AUC = 0.79), the differences were not statistically significant ($P = 0.094$ and $P = 0.069$, respectively;

Table 3 and Figure 2). Internal validation was performed using 1,000 bootstrap resamples. The bootstrap-corrected AUC was 0.85 (95% CI, 0.76–0.96). The calibration curve of the combined model demonstrated good agreement between the predicted and observed probabilities (*Figure 3*). DCA indicated a relatively high net benefit across a threshold probability range of 25%–75% (*Figure 4*).

2.3 Long-term Survival Outcomes

2.3.1 Determination of Cutoff Values for the Parameters

Among the factors evaluated for their association with PFS, SUVmax-T, FTV, TLF, and Max D had AUCs ≥ 0.60 and were categorized according to their optimal cutoff values, as prespecified in the analysis plan. Age, SUVmax-N, and SIR, which had AUCs < 0.60, were categorized according to their median values. Categorization of RE according to its optimal cutoff value resulted in complete separation and unstable model fitting; therefore, RE was categorized according to its median value instead (*Table 4*).

2.3.2 Survival Analysis

Univariable Cox regression analysis showed that SUVmax-T, MRI N stage, and rENE were significantly associated with PFS ($P < 0.05$). Multivariable survival analysis demonstrated that SUVmax-T and rENE were independent prognostic factors for PFS ($P < 0.05$) (*Table 5*). Based on the independent prognostic factors identified in the multivariable analysis, Kaplan–Meier survival curves showed that the 1-year PFS rates were 90.0% and 51.9% in the low- and high-SUVmax-T groups, respectively (P =

0.008), and 92.9% and 64.5% in patients without and with rENE, respectively (P = 0.006) (*Figure 5*).

2.4 Sankey Diagram Analysis

The Sankey diagrams visualized patient stratification based on imaging parameters, short-term treatment response, and long-term PFS status (*Figure 6*). *Figure 6a* shows the distribution of patients across eight subgroups defined by TLF, SIR, and rENE status. Patients with at least two low-risk parameters (TLF-Low, SIR-Low, or rENE-No) were more likely to achieve CR, whereas those with at least two high-risk parameters (TLF-High, SIR-High, or rENE-Yes) predominantly had Non-CR outcomes; notably, the subgroup with low TLF, low SIR, and positive rENE, most cases were still classified as Non-CR, despite the low-risk status of both TLF and SIR. In *Figure 6b*, the combination of SUVmax-T and rENE stratification was associated with differential PFS outcomes: patients with both parameters low-risk (SUVmax-T-Low, rENE-No) remained progression-free; those with one high-risk parameter had intermediate rates of disease progression; and those with both parameters high-risk (SUVmax-T-High, rENE-Yes) had the highest proportion of progression events. *Figure 6c* illustrates that all patients with CR remained progression-free, whereas a small subset of patients with Non-CR experienced disease progression.

3 Discussion

To our knowledge, this is the first study to integrate the complementary information provided by ^{18}F-FAPI PET/CT and MRI to investigate the predictive value of their

combination for short-term treatment response and long-term PFS in patients with NPC undergoing chemoradiotherapy. The results showed that the combined model achieved a numerically higher AUC than either single-modality model in predicting short-term CR. Regarding long-term outcomes, SUVmax-T ≥ 17.0 and the presence of rENE were both significantly associated with poorer PFS. These findings support the potential value and clinical utility of this multimodal approach for treatment response assessment and prognostic evaluation.

^{18}F-FAPI PET/CT targets FAP, and its derived parameters essentially reflect the degree of CAF activation and the burden of stromal remodeling within the tumor microenvironment [15]. Previous studies have demonstrated that ^{18}F-FAPI PET/CT-derived parameters, including SUVmax, FTV, and TLF, are associated with treatment response and survival in various malignancies, such as gastric cancer, pancreatic ductal adenocarcinoma, and peritoneal metastases [16-18]. However, the application of this technique to treatment response assessment in NPC remains in its early stages, with existing reports limited to small-sample follow-up studies [19] and preliminary investigations of sensitivity to immunotherapy [20]. Building on these findings, we further explored the clinical significance of these parameters in NPC. Our results showed that all parameters derived from ^{18}F-FAPI PET/CT could discriminate short-term CR, and that TLF was an independent predictor of short-term CR, supporting the aforementioned evidence. However, with respect to long-term outcomes, only SUVmax-T showed significant independent predictive value. This finding differs from

the conclusion of He et al. [16], who reported that volumetric parameters were superior to SUVmax. This discrepancy may be attributable to heterogeneity in tumor type, treatment regimen, follow-up duration, or sample size. Further validation in prospective, multicenter studies with larger sample sizes is warranted.

The SIR and rENE parameters obtained from conventional contrast-enhanced MRI (CE-MRI) complemented the functional information provided by PET/CT by characterizing vascular permeability and extranodal extension of lymph nodes, respectively. Dynamic contrast-enhanced MRI (DCE-MRI) parameters and MRI radiomic features have been shown to predict treatment response and survival outcomes in patients with NPC [21-23]. Our study further demonstrated that the SIR calculated from CE-MRI also has the potential to predict short-term treatment response, providing a simple and feasible imaging marker for clinical settings in which functional MRI parameters are unavailable. In the present study, the SIR was calculated as the ratio of the enhancement signal intensity of the tumor tissue to that of the contralateral medial pterygoid muscle and essentially reflected the degree of tumor vascularity and vascular permeability. Tumor angiogenesis is a critical process in tumor progression. High expression of vascular endothelial growth factor (VEGF) increases tumor microvessel density and promotes vascular immaturity and hyperpermeability [24]. These changes manifest as more pronounced signal enhancement on CE-MRI. Therefore, tumors with a higher SIR may exhibit more active angiogenesis, which may be associated with aggressive biological behavior and resistance to chemoradiotherapy [25].

As a morphological MRI feature, rENE directly reflects the biological behavior of tumor extension beyond the lymph node capsule into adjacent surrounding tissues and represents a high-risk sign for locoregional treatment failure and distant metastasis. The ninth edition of the AJCC/UICC TNM staging system for NPC has formally incorporated advanced rENE into the N3 category, thereby recognizing its adverse prognostic significance [26]. Studies by Mao et al. [27] and Tsai et al. [28] have further confirmed the prognostic value of rENE in terms of survival outcomes. Consistent with these findings, the present study demonstrated that rENE was not only a marker for long-term survival stratification but also a predictor of short-term response to chemoradiotherapy.

Although PET/CT can assess the tumor stromal burden, it cannot provide information on vascular permeability or lymph node capsule integrity. Conversely, although MRI offers excellent anatomical detail, it has limited ability to quantitatively assess the degree of stromal activation. Overcoming the limitations of single-modality imaging, this study integrated TLF, SIR, and rENE to establish, for the first time, a multimodal assessment system encompassing three major dimensions of malignant tumor biology: overall stromal burden, vascular permeability, and lymph node invasiveness. These parameters provide complementary information. TLF quantifies the overall stromal burden and reflects the extent of stromal remodeling and CAF activation [15]. SIR assesses vascular permeability and the degree of angiogenesis, thereby reflecting the vascular pathological basis of tumor invasiveness and treatment resistance

[25]. rENE directly depicts the anatomical abnormality of extranodal extension and indicates the risks of locoregional invasion and distant metastasis [26]. By integrating the three dimensions of the tumor microenvironment, vascular pathological characteristics, and anatomical invasiveness, this multimodal model enabled a comprehensive assessment of the overall malignant potential of the tumor.

The model validation results provided substantial evidence supporting the clinical value of the three-dimensional integrated framework. Although DeLong's test showed that the differences in AUC between the combined model (AUC = 0.88) and the PET/CT-only model (AUC = 0.76, P = 0.094) or the MRI-only model (AUC = 0.79, P = 0.069) did not reach statistical significance, the combined model showed better numerical performance in terms of accuracy (0.83 vs. 0.72 and 0.72), F1 score (0.80 vs. 0.67 and 0.73), and Brier score (0.13 vs. 0.19 and 0.19). After correction through bootstrap internal validation, the AUC of the combined model remained 0.85. Moreover, DCA indicated that the integrated model provided the greatest net clinical benefit across a relatively broad range of threshold probabilities. Taken together, these findings suggest that the fusion of multidimensional imaging information may enhance both the overall predictive performance and the clinical decision-making utility of the model, supporting the potential use of this framework as a pretreatment risk stratification tool for patients with NPC undergoing chemoradiotherapy.

Kaplan–Meier curves showed that patients with high SUVmax-T or the presence of rENE had significantly shorter PFS, facilitating pre-treatment stratification into high-

and low-risk groups and providing objective imaging-based evidence for the development of individualized treatment and follow-up strategies.

The Sankey diagram further illustrated the complementary value of ^{18}F-FAPI PET/CT and MRI parameters. For example, even among patients with comparable SUVmax-T levels, the rENE-positive subgroup showed a markedly higher proportion of flow toward progression (*Figure 6b*). This finding suggests that MRI-derived information on lymph node extracapsular extension may complement the limitations of PET-based functional parameters and help identify patients with a relatively low stromal burden in the primary tumor but a persistent risk of disease progression. An exception was the subgroup with low TLF and low SIR but positive rENE, in which most patients failed to achieve CR. This finding suggests that the parameters used in the combined stratification do not simply exert additive effects and that rENE may provide a stronger risk signal for assessing treatment response (*Figure 6a*). In addition, the Sankey diagram indicated that short-term CR was associated with a favorable prognosis and may partially reflect long-term survival outcomes.

This study has several limitations. First, it was a single-center retrospective study with a relatively limited sample size, and selection bias cannot be excluded. These findings should therefore be validated in future multicenter, large-scale prospective studies. Second, the retrospective design did not involve a fully standardized treatment protocol. Although all enrolled patients received platinum-based induction chemotherapy followed by IMRT, some heterogeneity existed in the specific treatment

regimens, including the number of cycles, drug doses, and the use of concomitant immunotherapy. This heterogeneity may have confounded clinical outcomes and consequently affected the observed associations between imaging parameters and prognosis. Third, although internal validation demonstrated good calibration, external validation in a larger patient cohort is warranted to further confirm the accuracy and generalizability of the model. Finally, the follow-up duration in this study was relatively short. Longer follow-up will be necessary to further clarify the long-term prognostic value of the model and the relevant imaging parameters.

In summary, integrating stromal burden parameters from ^{18}F-FAPI PET/CT with MRI-derived indicators of vascular permeability and lymph node invasion enables comprehensive capture of multidimensional malignant features. This multimodal integration demonstrated complementary value in both short-term treatment response assessment and long-term survival stratification, underscoring its potential for clinical application and supporting risk stratification before individualized treatment in patients with NPC.

Acknowledgements

No potential conflicts of interest were disclosed.

Author Contribution

Lingling Gao: Conceptualization, Data curation, Investigation, Methodology, Software, Visualization, Writing – original draft, Writing – review & editing. **Rui Yao:** Data curation, Investigation, Software, Validation. **Xiaolong Zheng:** Data curation, Formal analysis, Writing – review & editing. **Yujia Zhang:** Data curation. **Qingyou Ye:** Writing – review & editing. **Xinyan Zhang:** Writing – review & editing. **Ling Wang:** Conceptualization, Formal analysis, Investigation, Writing – review & editing. **Kun Tang:** Conceptualization, Formal analysis, Investigation, Methodology, Project administration, Supervision, Validation, Writing – review & editing.

Funding

No funding was procured for this work.

References

[1] Su ZY, Siak PY, Lwin YY, Cheah SC. Epidemiology of nasopharyngeal carcinoma: current insights and future outlook. Cancer Metastasis Rev 2024;43:919–39. https://doi.org/10.1007/s10555-024-10176-9.

[2] Cai M, Wang Y, Ma H, Yang L, Xu Z. Advances and challenges in immunotherapy for locally advanced nasopharyngeal carcinoma. Cancer Treat Rev 2024;131:102840. https://doi.org/10.1016/j.ctrv.2024.102840.

[3] Chen YP, Chan ATC, Le QT, Blanchard P, Sun Y, Ma J. Nasopharyngeal carcinoma. Lancet 2019;394:64–80. https://doi.org/10.1016/s0140-6736(19)30956-0.

[4] Zhang ERY, Neo JL, Chua MLK. Circulating Epstein-Barr virus DNA as a precision biomarker in nasopharyngeal carcinoma: from risk stratification to real-time treatment adaptation and disease surveillance. Curr Opin Oncol 2026;38:170–5. https://doi.org/10.1097/CCO.0000000000001231.

[5] Pajak W, Kleinrok J, Pec J, Orzechowski A, Drabko J, Sitarz R, et al. Therapeutic Innovations in Nasopharyngeal Carcinoma: Current Strategies and Emerging Perspectives. Life (Basel) 2026;16. https://doi.org/10.3390/life16050764.

[6] Chandekar KR, Prashanth A, Vinjamuri S, Kumar R. FAPI PET/CT Imaging-An Updated Review. Diagnostics (Basel) 2023;13. https://doi.org/10.3390/diagnostics13122018.

[7] Hamson EJ, Keane FM, Tholen S, Schilling O, Gorrell MD. Understanding fibroblast activation protein (FAP): substrates, activities, expression and targeting for cancer therapy. Proteomics Clin Appl 2014;8:454–63. https://doi.org/10.1002/prca.201300095.

[8] Sahai E, Astsaturov I, Cukierman E, DeNardo DG, Egeblad M, Evans RM, et al. A framework for advancing our understanding of cancer-associated fibroblasts. Nat Rev Cancer 2020;20:174–86. https://doi.org/10.1038/s41568-019-0238-1.

[9] Zhao L, Pang Y, Zheng H, Han C, Gu J, Sun L, et al. Clinical utility of [(68)Ga]Ga-labeled fibroblast activation protein inhibitor (FAPI) positron emission tomography/computed tomography for primary staging and recurrence detection in nasopharyngeal carcinoma. Eur J Nucl Med Mol Imaging 2021;48:3606–17. https://doi.org/10.1007/s00259-021-05336-w.

[10] Xu W, Zou Y, Zhang Y, Lv Q, Deng X, Li K, et al. The clinical value of FAPI PET/CT in delineating target volumes for nasopharyngeal carcinoma. Eur J Nucl Med Mol Imaging 2025;53:105–15. https://doi.org/10.1007/s00259-025-07347-3.

[11] Xu H, Lv W, Zhang H, Yuan Q, Wang Q, Wu Y, et al. Multimodality radiomics analysis based on [(18)F]FDG PET/CT imaging and multisequence MRI: application to nasopharyngeal carcinoma prognosis. Eur Radiol 2023;33:6677–88. https://doi.org/10.1007/s00330-023-09606-z.

[12] Kim HY, Choi JY, Park CH, Song MJ, Song DS, Kim CW, et al. Clinical factors predictive of insufficient liver enhancement on the hepatocyte-phase of Gd-EOB-

DTPA-enhanced magnetic resonance imaging in patients with liver cirrhosis. J Gastroenterol 2013;48:1180–7. https://doi.org/10.1007/s00535-012-0740-7.

[13] Yu H, Hai Y, Lu J. Exploratory high b value diffusion-weighted MR for quantitative differentiation of ileocecal inflammatory conditions and tumors. Insights Imaging 2025;16:41. https://doi.org/10.1186/s13244-025-01916-8.

[14] Eisenhauer EA, Therasse P, Bogaerts J, Schwartz LH, Sargent D, Ford R, et al. New response evaluation criteria in solid tumours: revised RECIST guideline (version 1.1). Eur J Cancer 2009;45:228–47. https://doi.org/10.1016/j.ejca.2008.10.026.

[15] Lode K, Kancherla S, Guttormsen Y, Berzaghi R, Maia VS, Moldes-Anaya A, et al. Preclinical evaluation of FAP-targeted PET imaging to investigate CAF responses to radiotherapy. Cancer Imaging 2026;26. https://doi.org/10.1186/s40644-026-01010-2.

[16] He H, Xie Y, Jiang C, Zhou W, Ye H. Prognostic Significance of Pretreatment [^{18}F]ALF-NOTA-FAPI-04 PET/CT in Patients With Recurrent Gastric Cancer Undergoing Combined PD-1 Inhibitor and Chemotherapy. Korean J Radiol 2026;27:264–75. https://doi.org/10.3348/kjr.2025.1458.

[17] Zhu Z, Cheng K, Yun Z, Zhang X, Hu X, Liu J, et al. [(18)F] AlF-NOTA-FAPI-04 PET/CT can predict treatment response and survival in patients receiving chemotherapy for inoperable pancreatic ductal adenocarcinoma. Eur J Nucl Med Mol Imaging 2023;50:3425–38. https://doi.org/10.1007/s00259-023-06271-8.

[18] Zhang Y, Xu M, Wang Y, Yu F, Chen X, Wang G, et al. Characteristics of (18)F-FAPI-04 PET/CT in patients with peritoneal metastasis and to predict treatment efficacy, a head-to-head comparison with (18)F-FDG PET/CT. Cancer Imaging 2025;25:66. https://doi.org/10.1186/s40644-025-00887-9.

[19] Jiang Y, Wen B, Li C, Tian Y, Xiao Z, Xu K, et al. The performance of (68)Ga-FAPI-04 PET/CT in head and neck squamous cell carcinoma: a prospective comparison with (18)F-FDG PET/CT. Eur J Nucl Med Mol Imaging 2023;50:2114–26. https://doi.org/10.1007/s00259-023-06138-y.

[20] Li N, Sun F, Zheng H, Zhao J, Sun B, Sui F. 425P 18F-FAPI PET/CT imaging to explore the evaluation of immunotherapy efficacy in HNSCC. Ann Oncol 2024;35. https://doi.org/10.1016/j.annonc.2024.10.448.

[21] Kou J, Peng JY, Lv WB, Wu CF, Chen ZH, Zhou GQ, et al. A Serial MRI-based Deep Learning Model to Predict Survival in Patients with Locoregionally Advanced Nasopharyngeal Carcinoma. Radiol Artif Intell 2025;7:e230544. https://doi.org/10.1148/ryai.230544.

[22] Qin Y, Yu X, Hou J, Hu Y, Li F, Wen L, et al. Prognostic Value of the Pretreatment Primary Lesion Quantitative Dynamic Contrast-Enhanced Magnetic Resonance Imaging for Nasopharyngeal Carcinoma. Acad Radiol 2019;26:1473–82. https://doi.org/10.1016/j.acra.2019.01.021.

[23] Li H, Huang W, Wang S, Balasubramanian PS, Wu G, Fang M, et al. Comprehensive integrated analysis of MR and DCE-MR radiomics models for

prognostic prediction in nasopharyngeal carcinoma. Vis Comput Ind Biomed Art 2023;6:23. https://doi.org/10.1186/s42492-023-00149-0.

[24] Zeng Y, Fu BM. Angiogenesis and Microvascular Permeability. Cold Spring Harb Perspect Med 2025;15. https://doi.org/10.1101/cshperspect.a041163.

[25] Xia C, Zhao J, Huang Y, Miao H, Zhao F. Angiogenesis in nasopharyngeal carcinoma: insights, imaging, and therapeutic strategies. Front Oncol 2024;14:1331064. https://doi.org/10.3389/fonc.2024.1331064.

[26] Pan JJ, Mai HQ, Ng WT, Hu CS, Li JG, Chen XZ, et al. Ninth Version of the AJCC and UICC Nasopharyngeal Cancer TNM Staging Classification. JAMA Oncol 2024;10:1627–35. https://doi.org/10.1001/jamaoncol.2024.4354.

[27] Mao Y, Wang S, Lydiatt W, Shah JP, Colevas AD, Lee AWM, et al. Unambiguous advanced radiologic extranodal extension determined by MRI predicts worse outcomes in nasopharyngeal carcinoma: Potential improvement for future editions of N category systems. Radiother Oncol 2021;157:114–21. https://doi.org/10.1016/j.radonc.2021.01.015.

[28] Tsai TY, Chou YC, Lu YA, Kang CJ, Huang SF, Liao CT, et al. The prognostic value of radiologic extranodal extension in nasopharyngeal carcinoma: Systematic review and meta-analysis. Oral Oncol 2021;122:105518. https://doi.org/10.1016/j.oraloncology.2021.105518.

Figure Legends

Figure 1 Flowchart for the selection of patients in the study. FAPI, fibroblast activation protein inhibitor; PET/CT, positron emission tomography/computed tomography; MRI, magnetic resonance imaging.

Figure 2 ROC curves of three models for predicting short-term CR.

Figure 3 Calibration curve of the multimodal combined model. The x-axis represents the model-predicted probability of response, and the y-axis indicates the actual observed probability within the patient cohort. Apparent: the initial performance of the model prior to any statistical correction; Bias-corrected: the true calibration accuracy after bias adjustment via resampling techniques; Ideal: the boundary of perfect prediction under optimal conditions.

Figure 4 Decision curve analysis of three models for predicting short-term CR.

Figure 5 Kaplan–Meier survival curves for independent imaging biomarkers associated with PFS, including SUVmax-T and rENE. SUVmax-T, maximum standardized uptake value of the primary tumor; rENE, radiologic extranodal extension.

Figure 6 Sankey diagram illustrating patient flow across independent imaging biomarkers, short-term response, and PFS. The left panel (a) depicts the flow of independent prognostic factors to short-term response, the middle panel (b) depicts the flow of independent prognostic factors to PFS, and the right panel (c) depicts the flow from short-term response to PFS. TLF, total lesion fibroblast activation protein

expression; SIR, signal intensity ratio; rENE, radiologic extranodal extension; SUVmax-T, maximum standardized uptake value of the primary tumor.

Table 1 Characteristics of patients and comparison between CR and Non-CR patients

Characteristic	Total (n = 46)	CR (n = 19)	Non-CR (n = 27)	P
SIR	2.12 ± 0.43	1.99 ± 0.39	2.22 ± 0.44	0.083
Age (years)	55.00 (41.25, 64.75)	53.00 (42.00, 59.00)	57.00 (41.00, 72.00)	0.199
SUVmax-T	13.83 (11.22, 16.13)	12.65 (9.50, 14.36)	14.88 (12.13, 18.94)	0.011
FTV (cm^3)	7.71 (5.58, 11.68)	5.64 (4.48, 7.71)	9.22 (6.12, 18.55)	0.011
TLF	62.05 (32.47, 109.00)	41.23 (14.86, 66.02)	85.72 (51.67, 208.64)	0.002
SUVmax-N	10.09 (4.42, 13.55)	4.82 (0.00, 10.31)	12.82 (8.46, 14.66)	< 0.001
Max D (mm)	24.50 (19.25, 34.75)	22.00 (20.00, 29.50)	25.00 (19.00, 38.00)	0.517
RE (%)	63.93 (15.57, 175.44)	99.05 (12.77, 122.47)	46.01 (16.79, 198.99)	0.547
Sex				0.729
Female	18 (39.13)	8 (42.11)	10 (37.04)	
Male	28 (60.87)	11 (57.89)	17 (62.96)	
TNM stage				0.051
II	7 (15.22)	5 (26.32)	2 (7.41)	
III	23 (50.00)	11 (57.89)	12 (44.44)	
IV	16 (34.78)	3 (15.79)	13 (48.15)	
MRI T stage				0.068
T1	4 (8.70)	4 (21.05)	0 (0.00)	
T2	13 (28.26)	6 (31.58)	7 (25.93)	
T3	21 (45.65)	6 (31.58)	15 (55.56)	
T4	8 (17.39)	3 (15.79)	5 (18.52)	
MRI N stage				0.006
N0	8 (17.39)	6 (31.58)	2 (7.41)	
N1	7 (15.22)	5 (26.32)	2 (7.41)	
N2	15 (32.61)	6 (31.58)	9 (33.33)	
N3	16 (34.78)	2 (10.53)	14 (51.85)	
rENE				0.007
No	31 (67.39)	17 (89.47)	14 (51.85)	
Yes	15 (32.61)	2 (10.53)	13 (48.15)	

Data are presented as mean ± standard deviation, number (percentage), and median [interquartile range]. CR=complete response, Non-CR=non-complete response, SIR=lesion-to-muscle signal intensity ratio, SUVmax-T=maximum standardized uptake value of the primary tumor, FTV=FAPI-avid tumor volume, TLF=total lesion fibroblast activation protein expression, SUVmax-N=maximum standardized uptake value of the metastatic neck lymph node, Max D=maximum tumor diameter, RE=relative signal enhancement rate, TNM=tumor-node-metastasis, rENE=radiologic extranodal extension.

Table 2 Univariable and multivariable logistic regression analyses of clinical variables, MRI, and ^{18}F-FAPI PET/CT parameters for predicting short-term CR

Variables	Univariate analysis		Multivariate analysis	
	OR (95% CI)	P	OR (95% CI)	P
Age (years)	1.02 (0.98–1.07)	0.255		
Sex				
Female	1.00 (Reference)			
Male	1.24 (0.37–4.10)	0.729		
TNM stage				
II	1.00 (Reference)		1.00 (Reference)	
III	2.73 (0.44–17.05)	0.283	0.91 (0.09–9.10)	0.933
IV	10.83 (1.37–85.44)	0.024	6.31 (0.53–74.83)	0.145
MRI T stage				
T1-T2	1.00 (Reference)			
T3-T4	3.89 (1.08–13.96)	0.037		
MRI N stage				
N0-N1	1.00 (Reference)			
N2-N3	7.91 (1.95–32.02)	0.004		
SUVmax-T	1.23 (1.05–1.45)	0.013		
TLF	1.02 (1.01–1.04)	0.019	1.03 (1.01–1.05)	0.027
SUVmax-N	1.21 (1.06–1.37)	0.003		
Max D (mm)	1.03 (0.97–1.09)	0.294		
RE (%)	1.00 (1.00–1.01)	0.416		
SIR	3.92 (0.81–19.10)	0.090	14.41 (1.56–133.54)	0.019
rENE				
No	1.00 (Reference)		1.00 (Reference)	
Yes	7.89 (1.52–41.02)	0.014	11.06 (1.17–104.48)	0.036

OR=odds ratio, CI=confidence interval, TNM=tumor-node-metastasis, SUVmax-T=maximum standardized uptake value of the primary tumor, TLF=total lesion fibroblast activation protein expression, SUVmax-N=maximum standardized uptake value of the metastatic neck lymph node, Max D=maximum tumor diameter, RE=relative signal enhancement rate, SIR=lesion-to-muscle signal intensity ratio, rENE=radiologic extranodal extension.

Table 3 Comparison of prognostic performance of PET/CT, MRI, and combined models for short-term CR

Model	Predictor	AUC (95%CI)	Accuracy (95%CI)	Sensitivity (95%CI)	Specificity (95%CI)	F1 score	Brier score	P vs Combined
PET/CT Model	TLF	0.76 (0.62–0.90)	0.72 (0.57–0.84)	0.68 (0.48–0.89)	0.74 (0.58–0.91)	0.67	0.19	0.094
MRI Model	SIR, rENE	0.79 (0.65–0.92)	0.72 (0.57–0.84)	0.95 (0.85–1.00)	0.56 (0.37–0.74)	0.73	0.19	0.069
Combined Model	TLF, SIR, rENE	0.88 (0.77–0.98)	0.83 (0.69–0.92)	0.84 (0.68–1.00)	0.81 (0.67–0.96)	0.80	0.13	–

TLF=total lesion fibroblast activation protein expression, SIR=lesion-to-muscle signal intensity ratio, rENE=radiologic extranodal extension, AUC=area under the curve, CI=confidence interval, F1 score=harmonic mean of precision and recall, Brier score=mean squared error between predicted probabilities and observed outcomes.

Table 4 Cutoff values related to PFS and their diagnostic efficacy

Variables	PFS				
	Cutoff value	Accuracy (95%CI)	Sensitivity (95%CI)	Specificity (95%CI)	AUC (95% CI)
Age (years)	51.5	0.46 (0.31–0.61)	0.41 (0.26–0.56)	0.71 (0.38–1.00)	0.51 (0.26–0.76)
SUVmax-T	17.035	0.78 (0.64–0.89)	0.82 (0.70–0.94)	0.57 (0.20–0.94)	0.60 (0.32–0.87)
FTV (cm^3)	7.823	0.63 (0.48–0.77)	0.59 (0.44–0.74)	0.86 (0.60–1.00)	0.69 (0.48–0.89)
TLF	76.261	0.65 (0.50–0.79)	0.64 (0.49–0.79)	0.71 (0.38–1.00)	0.67 (0.45–0.88)
SUVmax-N	7.762	0.48 (0.33–0.63)	0.41 (0.26–0.56)	0.86 (0.60–1.00)	0.55 (0.33–0.76)
Max D (mm)	16.5	0.17 (0.08–0.31)	0.10 (0.01–0.20)	0.57 (0.20–0.94)	0.65 (0.41–0.89)
RE (%)	143.102	0.57 (0.41–0.71)	0.67 (0.52–0.81)	0.00 (0.00–0.00)	0.64 (0.44–0.83)
SIR	1.965	0.50 (0.35–0.65)	0.44 (0.28–0.59)	0.86 (0.60–1.00)	0.51 (0.26–0.76)

PFS=progression-free survival, SUVmax-T=maximum standardized uptake value of the primary tumor, FTV=FAPI-avid tumor volume, TLF=total lesion fibroblast activation protein expression, SUVmax-N=maximum standardized uptake value of the metastatic neck lymph node, Max D=maximum tumor diameter, RE=relative signal enhancement rate, SIR=lesion-to-muscle signal intensity ratio, CI=confidence interval, AUC=area under the curve.

Table 5 Univariable and multivariable Cox proportional hazards regression analysis for PFS

Variables	Univariate analysis		Multivariate analysis	
	HR (95%CI)	P	HR (95%CI)	P
Age (years)				
<55	1.00 (Reference)			
≥55	1.26 (0.28–5.65)	0.760		
Sex				
Female	1.00 (Reference)			
Male	4.32 (0.52–35.90)	0.176		
TNM stage				
II	1.00 (Reference)			
III	1.00 (0.10–9.61)	0.999		
IV	1.50 (0.16–14.40)	0.728		
MRI T stage				
T1-T2	1.00 (Reference)			
T3-T4	3.56 (0.43–29.57)	0.240		
MRI N stage				
N0-N2	1.00 (Reference)			
N3	6.22 (1.20–32.29)	0.030		
SUVmax-T				
<17.0	1.00 (Reference)		1.00 (Reference)	
≥17.0	6.06 (1.33–27.55)	0.020	6.97 (1.46–33.27)	0.015
FTV (cm^3)				
<7.8	1.00 (Reference)			
≥7.8	7.40 (0.89–61.55)	0.064		
TLF				
<76.3	1.00 (Reference)			
≥76.3	3.84 (0.74–19.82)	0.108		
SUVmax-N				
<10.1	1.00 (Reference)			
≥10.1	1.47 (0.33–6.57)	0.614		
Max D (mm)				
<16.5	1.00 (Reference)			
≥16.5	0.25 (0.06–1.11)	0.069		
RE (%)				
<63.93	1.00 (Reference)			
≥63.93	0.76 (0.17–3.38)	0.713		
SIR				
<2.0	1.00 (Reference)			
≥2.0	1.32 (0.29–5.95)	0.715		
rENE				
No	1.00 (Reference)		1.00 (Reference)	

Yes	7.22 (1.39–37.61)	0.019	8.12 (1.51–43.64)	0.015

HR=hazard ratio, CI=confidence interval, TNM=tumor-node-metastasis, SUVmax-T=maximum standardized uptake value of the primary tumor, FTV=FAPI-avid tumor volume, TLF=total lesion fibroblast activation protein expression, SUVmax-N=maximum standardized uptake value of the metastatic neck lymph node, Max D=maximum tumor diameter, RE=relative signal enhancement rate, SIR=lesion-to-muscle signal intensity ratio, rENE=radiologic extranodal extension.

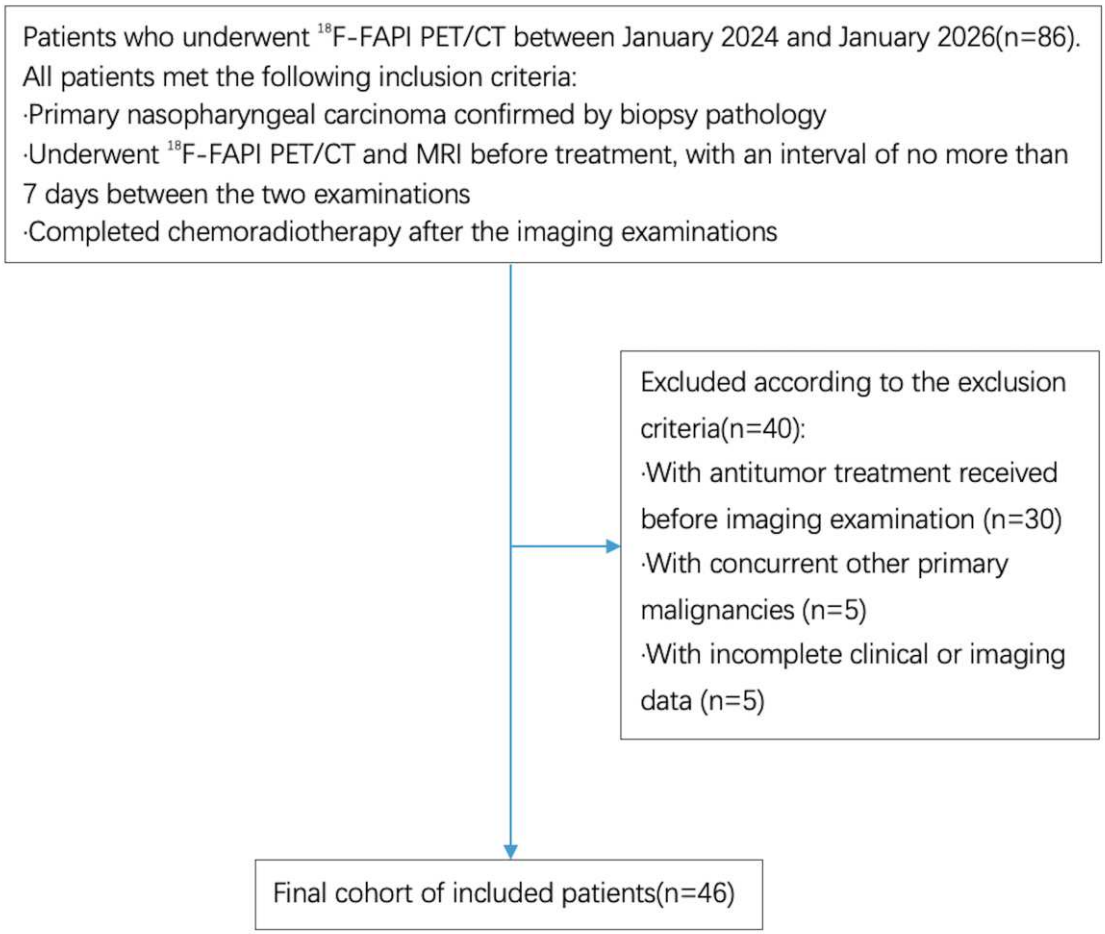


Figure 1 Flowchart for the selection of patients in the study. FAPI, fibroblast activation protein inhibitor; PET/CT, positron emission tomography/computed tomography; MRI, magnetic resonance imaging

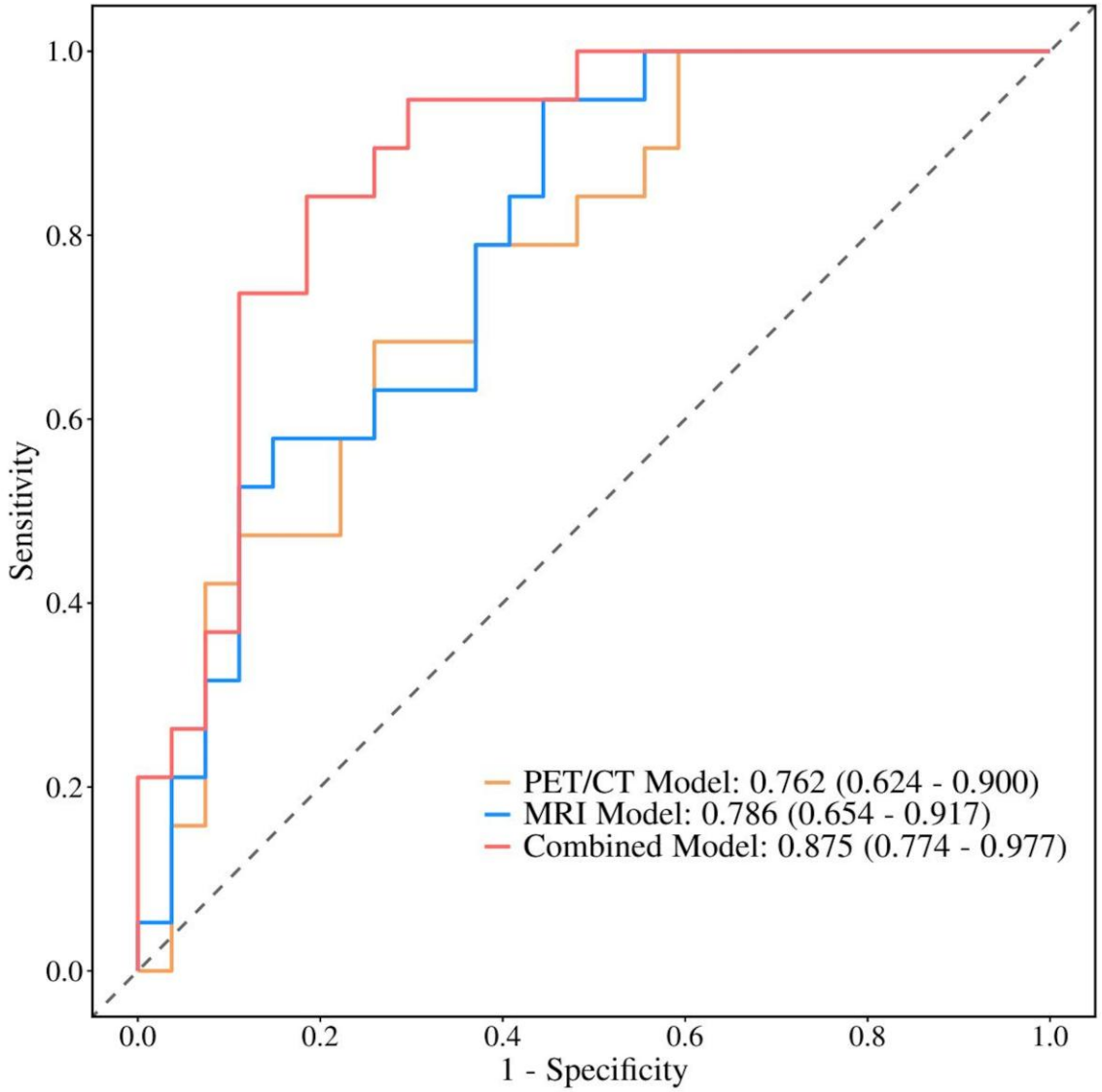


Figure 2 ROC curves of three models for predicting short-term CR

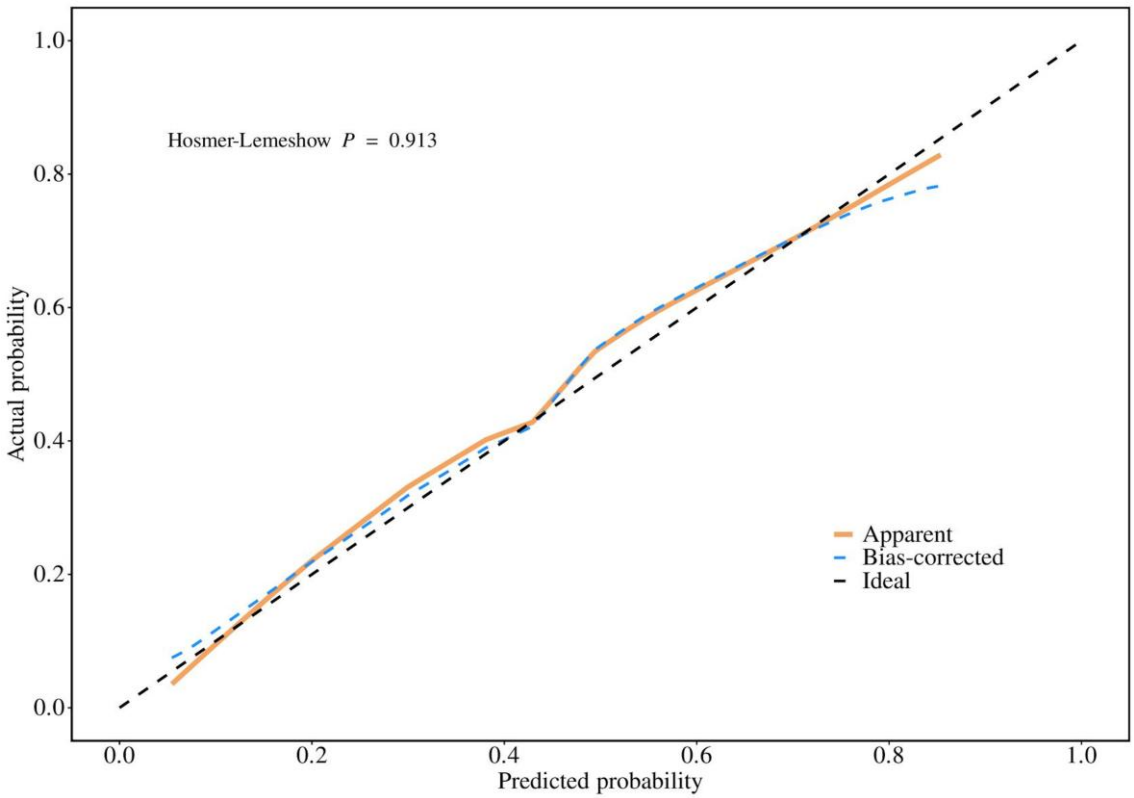


Figure 3 Calibration curve of the multimodal combined model

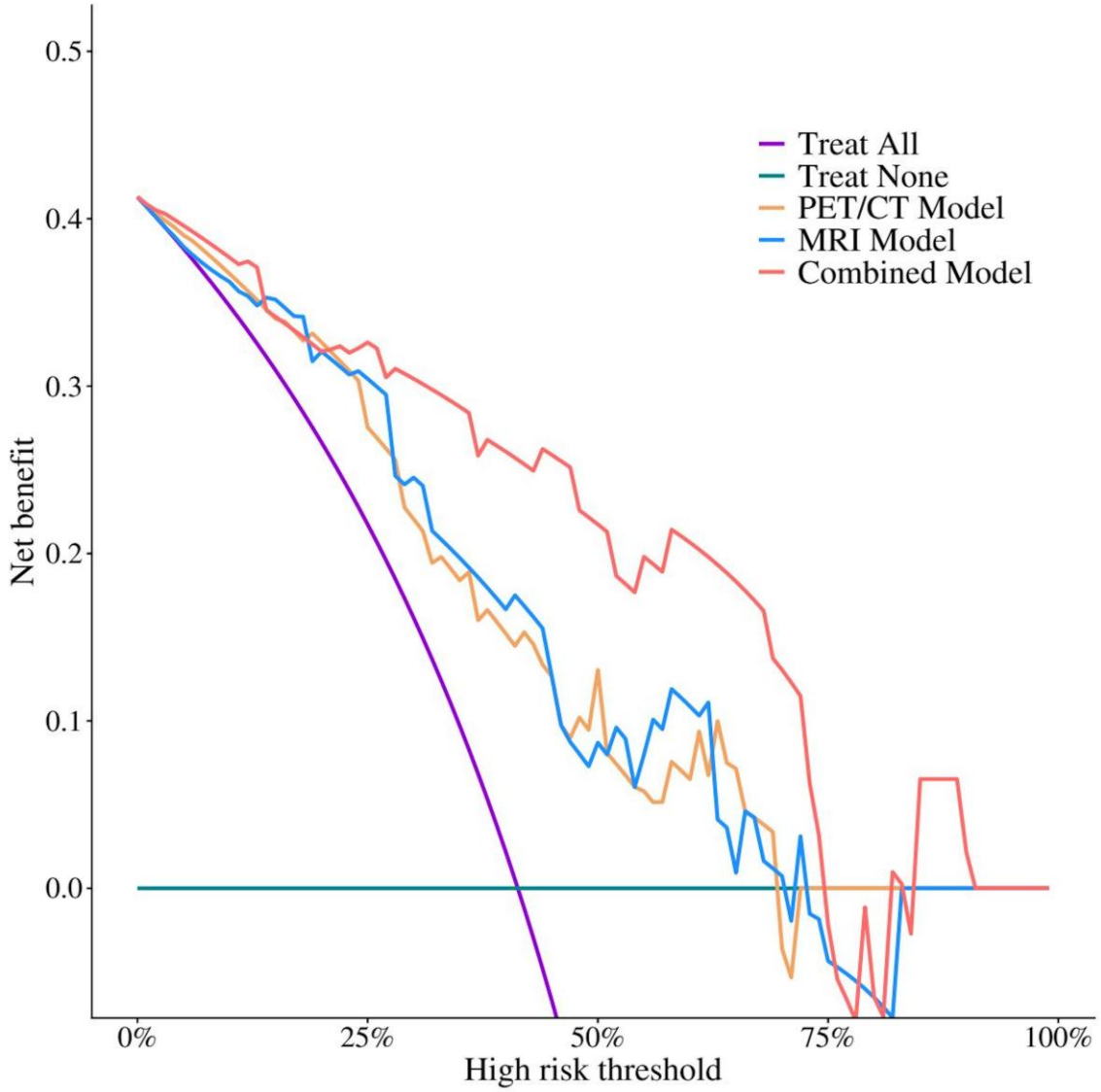


Figure 4 Decision curve analysis of three models for predicting short-term CR

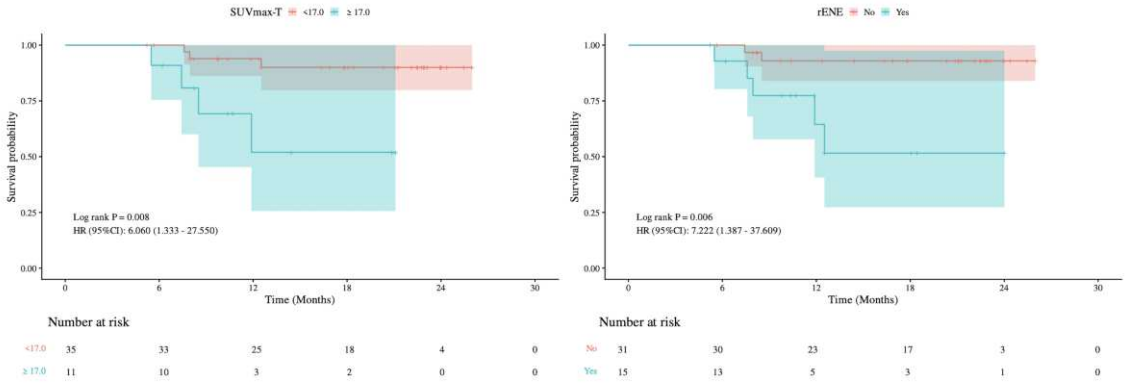


Figure 5 Kaplan–Meier survival curves for independent imaging biomarkers associated with PFS, including SUVmax-T and rENE

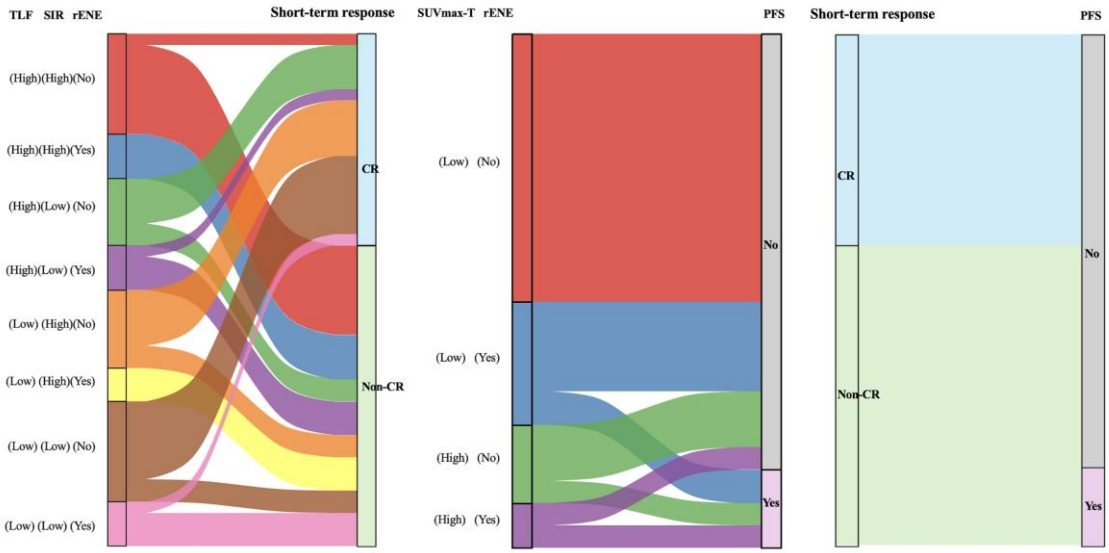


Figure 6 Sankey diagram illustrating patient flow across independent imaging biomarkers, short-term response, and PFS